

## Article

# Physicochemical Features and NH<sub>3</sub>-SCR Catalytic Performance of Natural Zeolite Modified with Iron—The Effect of Fe Loading

Magdalena Saramok <sup>1,\*</sup>, Marek Inger <sup>1,\*</sup>, Katarzyna Antoniak-Jurak <sup>1</sup>, Agnieszka Szymaszek-Wawryca <sup>2</sup>,  
Bogdan Samojeden <sup>2</sup> and Monika Motak <sup>2</sup>

<sup>1</sup> Łukasiewicz Research Network—New Chemical Syntheses Institute, Al. Tysiąclecia Państwa Polskiego 13a, 24-110 Puławy, Poland; katarzyna.antoniak@ins.lukasiewicz.gov.pl

<sup>2</sup> Faculty of Energy and Fuels, AGH University of Science and Technology, Al. Mickiewicza 30, 30-059 Kraków, Poland; agnszym@agh.edu.pl (A.S.-W.); bsamo1@agh.edu.pl (B.S.); motakm@agh.edu.pl (M.M.)

\* Correspondence: magdalena.saramok@ins.lukasiewicz.gov.pl (M.S.); marek.inger@ins.lukasiewicz.gov.pl (M.I.)

**Abstract:** In modern dual-pressure nitric acid plants, the tail gas temperature usually exceeds 300 °C. The NH<sub>3</sub>-SCR catalyst used in this temperature range must be resistant to thermal deactivation, so commercial vanadium-based systems, such as V<sub>2</sub>O<sub>5</sub>-WO<sub>3</sub> (MoO<sub>3</sub>)-TiO<sub>2</sub>, are most commonly used. However, selectivity of this material significantly decreases above 350 °C due to the increase in the rate of side reactions, such as oxidation of ammonia to NO and formation of N<sub>2</sub>O. Moreover, vanadium compounds are toxic for the environment. Thus, management of the used catalyst is complicated. One of the alternatives to commercial V<sub>2</sub>O<sub>5</sub>-TiO<sub>2</sub> catalysts are natural zeolites. These materials are abundant in the environment and are thus relatively cheap and easily accessible. Therefore, the aim of the study was to design a novel iron-modified zeolite catalyst for the reduction of NO<sub>x</sub> emission from dual-pressure nitric acid plants via NH<sub>3</sub>-SCR. The aim of the study was to determine the influence of iron loading in the natural zeolite-supported catalyst on its catalytic performance in NO<sub>x</sub> conversion. The investigated support was firstly formed into pellets and then impregnated with various contents of Fe precursor. Physicochemical characteristics of the catalyst were determined by XRF, XRD, low-temperature N<sub>2</sub> sorption, FT-IR, and UV-Vis. The catalytic performance of the catalyst formed into pellets was tested on a laboratory scale within the range of 250–450 °C using tail gases from a pilot nitric acid plant. The results of this study indicated that the presence of various iron species, including natural isolated Fe<sup>3+</sup> and the introduced Fe<sub>x</sub>O<sub>y</sub> oligomers, contributed to efficient NO<sub>x</sub> reduction, especially in the high-temperature range, where the NO<sub>x</sub> conversion rate exceeded 90%.

**Keywords:** nitric acid plant; selective catalytic reduction; clinoptilolite; iron-modified zeolite catalyst



**Citation:** Saramok, M.; Inger, M.; Antoniak-Jurak, K.; Szymaszek-Wawryca, A.; Samojeden, B.; Motak, M. Physicochemical Features and NH<sub>3</sub>-SCR Catalytic Performance of Natural Zeolite Modified with Iron—The Effect of Fe Loading. *Catalysts* **2022**, *12*, 731. <https://doi.org/10.3390/catal12070731>

Academic Editor: Anker Degn Jensen

Received: 18 May 2022

Accepted: 28 June 2022

Published: 1 July 2022

**Publisher's Note:** MDPI stays neutral with regard to jurisdictional claims in published maps and institutional affiliations.

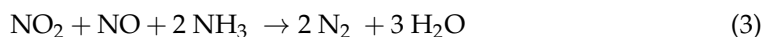
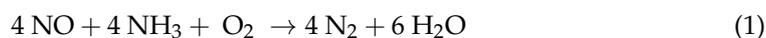


**Copyright:** © 2022 by the authors. Licensee MDPI, Basel, Switzerland. This article is an open access article distributed under the terms and conditions of the Creative Commons Attribution (CC BY) license (<https://creativecommons.org/licenses/by/4.0/>).

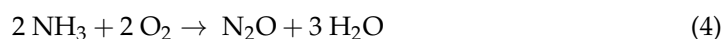
## 1. Introduction

NO<sub>x</sub> emitted from stationary (power plants, nitric acid, or adipic acid production) and mobile sources are treated as a serious environmental problem. They contribute to the formation of acid rain and photochemical smog and cause deterioration of water and soil quality [1]. Therefore, it is highly necessary to reduce industrial NO<sub>x</sub> emissions. The method of NO<sub>x</sub> abatement is usually correlated with the emission origin. In the plants, which produce nitric acid, high-efficiency absorption, non-selective catalytic reduction (NSCR), selective catalytic reduction (SCR), and absorption in sodium hydroxide solution can be used [2]. Among them, selective catalytic reduction with ammonia (NH<sub>3</sub>-SCR) is

the most efficient. The process involves selective reduction of  $\text{NO}_x$  with  $\text{NH}_3$  to form  $\text{N}_2$  and  $\text{H}_2\text{O}$ , as presented by Equations (1)–(3):



Ammonia, used as the reducing agent, is easily available in nitric acid plants since it is a substrate in the production of  $\text{HNO}_3$ . Typically, the SCR reactor is installed at the end of the technological line and does not significantly affect the production of acid. Therefore,  $\text{NH}_3$ -SCR can be used in most existing nitric acid plants. The catalyst used in the  $\text{NH}_3$ -SCR process is required to exhibit high activity in low- and high-temperature regions, satisfactory selectivity to  $\text{N}_2$ , and good thermal stability. In fact, these requirements are met by metal oxide systems, such as the commercial catalyst  $\text{V}_2\text{O}_5\text{-WO}_3$  ( $\text{MoO}_3$ )- $\text{TiO}_2$  [3]. However, the material is not free from some important drawbacks, such as the toxicity of vanadium compounds. Moreover, selectivity of the catalysts above  $350^\circ\text{C}$  is limited by the side reactions described by Equations (4) and (5):



Due to the above-mentioned problems, a number of materials have been investigated as the alternative catalysts of  $\text{NH}_3$ -SCR [4–7]. According to the study reported by Kobayashi et al. [8], application of  $\text{TiO}_2$  does not provide sufficient dispersion of the active phase, surface acidity, and thermal stability of the catalyst. Therefore, further research has shifted to alternative supports of the novel catalyst. Among them, natural zeolites were found to be very promising precursors of the novel catalysts [9,10]. The great advantage of these materials is their abundance in the environment and thus their relatively low price, which is very beneficial for industrial applications. The representative of natural zeolites is clinoptilolite, belonging to the heulandite (HEU) family [11]. The material shows strongly acidic character, determined by its Si/Al molar ratio of ca. 4, its well-developed pore system, and its thermal stability. According to the Eley–Rideal mechanism,  $\text{NH}_3$ -SCR assumes simultaneous adsorption of alkaline  $\text{NH}_3$  and neutral  $\text{NO}$  and their interaction on the catalyst surface [12]. Therefore, high concentration of acid centers delivered by clinoptilolite improves ammonia adsorption capacity and  $\text{NH}_3$ -SCR reaction rate. Moreover, clinoptilolite provides good ion exchange capacity, and as a consequence, its acidic character can be easily elevated by acid pretreatment [13]. Additionally, the presence of micro- and mesopores in the zeolitic structure facilitates the diffusion of gas molecules through the catalyst's pores and easy access to active centers. Lastly, clinoptilolite belongs to the residual materials, usually stored on heaps. Therefore, its recycling is in agreement with the assumptions of circular economy. All in all, the above-mentioned properties make clinoptilolite a promising candidate for the precursor of a new catalyst of  $\text{NH}_3$ -SCR [13–15]. To date, research on the application of clinoptilolite was mostly limited to SCR with hydrocarbons as reducing agents. Ghasemian et al. [16] proved that protonated clinoptilolite is a promising precursor of a new catalyst of SCR with methane as a reducing agent. Another study conducted by the authors [15,17] concerned clinoptilolite as a possible support for the catalyst of SCR with propane. However, only few studies have explored zeolite as a support for SCR with ammonia [13,18].

Another important issue in the design of a novel  $\text{NH}_3$ -SCR catalyst is the active phase. Over recent years, the focus of researchers has shifted to systems with transition metals, especially iron [5,12,19,20]. The choice of Fe was motivated by its environmentally benign characteristics, low price, and prominent thermal stability. Additionally, iron catalysts exhibit excellent medium- and high-temperature activity and satisfactory selectivity to  $\text{N}_2$ .

Moreover, the facile redox equilibrium,  $\text{Fe}^{3+} \leftrightarrow \text{Fe}_3\text{O}_4 \leftrightarrow \text{Fe}^{2+}$ , contributes to high oxygen storage capacity, which is very beneficial for SCR catalysts.

Highly satisfactory activity of iron-modified clinoptilolite in SCR with ammonia was confirmed in the previous study [18]. It was found that raw clinoptilolite in a form of fine grain showed 30% of NO conversion in the range of 350–450 °C. The high efficiency of the material in  $\text{NH}_3$ -SCR with the gas mixture reflecting the industrial composition was also confirmed. It was observed that at 400 °C,  $\text{NO}_x$  conversion for Fe-clinoptilolite exceeded 80%, and high selectivity to  $\text{N}_2$  was preserved in the entire temperature range. Additionally, 82% NO conversion was obtained for the previously shaped iron-modified clinoptilolite. In conditions similar to industrial ones, the highest catalytic activity was obtained above 400 °C, and these temperatures also maintained very favorable selectivity towards  $\text{N}_2$ . Importantly, no formation of  $\text{N}_2\text{O}$  was observed during the catalytic reaction.

In this work, the aim was to investigate the influence of iron loading on the low- and high-temperature catalytic performance of Fe-modified clinoptilolite formed into pellets. In this research, iron was considered the active phase since this transition metal exhibits outstanding redox properties and, at the same time, neutrality to the environment. Therefore, the experiments will contribute to the development of more ecologically friendly catalysts of the  $\text{NH}_3$ -SCR process. Moreover, in the experiments, a real tail gas mixture, which normally enters SCR reactors in nitric acid plants, was used. To the best of our knowledge, no one so far has investigated the catalytic performance of such material under near-industrial conditions. Thus, this work makes a significant contribution to the field of low-price and nontoxic industrial catalysts of  $\text{NH}_3$ -SCR.

## 2. Results and Discussion

### 2.1. Physicochemical Properties of the Materials

#### 2.1.1. Chemical Composition, Crystal Structure, and Morphology of the Materials

The chemical compositions of raw (Clin), protonated (H-Clin), and Fe-modified clinoptilolite (Fe-Clin-1, 2, or 3) are presented in Table 1. The crystalline structure of the materials was analyzed using XRD, and the obtained patterns are shown in Figure 1.

**Table 1.** Chemical composition (in wt.%) of the analyzed materials determined by XRF.

Sample	$\text{Fe}_2\text{O}_3$ (%)	$\text{SiO}_2$ (%)	$\text{Al}_2\text{O}_3$ (%)	$\text{Na}_2\text{O}$ (%)	$\text{MgO}$ (%)	$\text{SO}_3$ (%)	$\text{K}_2\text{O}$ (%)	$\text{CaO}$ (%)	$\text{TiO}$ (%)	$\text{MnO}$ (%)
Clin	2.1	74.7	12.1	0.8	0.8	0.04	3.2	3.7	0.2	0.07
H-Clin	2.0	80.5	11.4	0.1	0.7	0.03	3.0	1.7	0.2	0.03
Fe-Clin-1	8.6	71.0	10.1	0.1	0.6	5.00	2.6	1.5	0.2	0.01
Fe-Clin-2	11.1	69.2	10.0	0.1	0.5	4.59	2.5	1.5	0.2	0.01
Fe-Clin-3	11.9	66.7	9.4	0.1	0.5	7.41	2.3	1.2	0.2	0.01

As presented in Table 1, the raw clinoptilolite consisted mainly of  $\text{SiO}_2$  and  $\text{Al}_2\text{O}_3$  and contained some additives of other alkaline metal oxides. Additionally, the analysis provided strong evidence of the presence of iron oxide in the natural zeolite. After protonation, the percentage contribution of  $\text{SiO}_2$  increased with a simultaneous slight decrease of  $\text{Al}_2\text{O}_3$  content. This result is in line with that obtained by Burris and Juenger [21], who ascribed the decrease in aluminum content to partial dealumination of the material or its dissolution in acidic medium. However, since the XRD pattern of H-Clin corresponded to that of Clin, the degrading influence of the acid can be excluded. After the deposition of iron, the detected content of  $\text{Fe}_2\text{O}_3$  significantly increased, proving efficient incorporation of various iron species into the zeolite structure. However, it can be also observed that after the third impregnation, the amount of  $\text{Fe}_2\text{O}_3$  was very close to that obtained after the second impregnation. Additionally, the catalysts contained considerable amounts of  $\text{SO}_3$  as the result of using  $\text{FeSO}_4$  as the precursor of iron. Therefore, the applied calcination temperature was probably insufficient to provide effective decomposition of the salt deposited on the zeolite matrix.

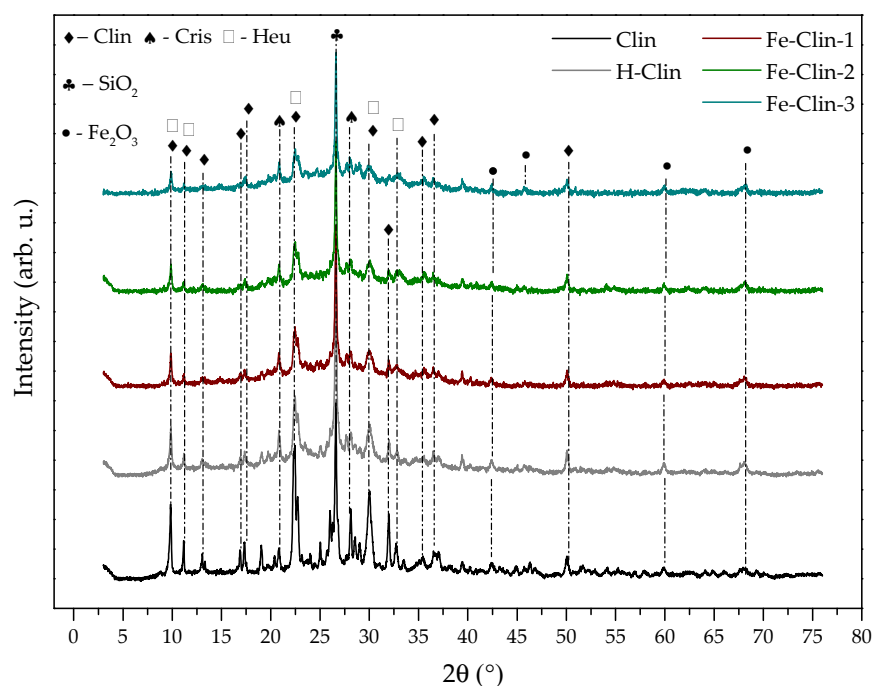


**Figure 1.** XRD patterns obtained for raw clinoptilolite (Clin), protonated clinoptilolite (H-Clin), and clinoptilolite modified with iron (Fe-Clin-1, Fe-Clin-2, Fe-Clin-3).

According to the results of XRD, the analyzed sample consisted mainly of heulandite/c clinoptilolite, confirmed by the diffraction maxima at  $2\theta$  of 9.8, 11.4, 12.9, 16.8, 17.4, 20.7, 22.6, 30.0, 32.0, 32.9, 35.5, 36.7, and  $50.3^\circ$ . The reflection at  $2\theta$  of  $26.6^\circ$  corresponds to  $\text{SiO}_2$ , while those at  $21.9$  and  $28.1^\circ$  are due to the presence of cristobalite impurities in the solid [13]. The observed diffraction maxima are in good agreement with those reported in the literature [18,22]. The comparative analysis of the materials showed that protonation by acid treatment did not result in any noticeable structural changes. However, some of the diffraction maxima exhibited lower intensity or completely disappeared, indicating decreased crystallinity of the catalysts compared to the raw zeolite.

After modification with iron, the positions of diffraction maxima characteristic of the clinoptilolite phase remained unchanged. Thus, deposition of the active phase did not cause any significant damage to the structure. However, the intensity of the reflections was the lowest for the material with the highest concentration of iron. Larger aggregates of  $\text{Fe}_2\text{O}_3$  on the zeolite surface can potentially be present at  $2\theta$  of  $42.0$ ,  $45.8$ ,  $60.2$ , and  $68.2^\circ$  [23]. However, apart from bigger particles, iron also isomorphously substituted for aluminum in the zeolite framework and thus was impossible to be detected by XRD technique. The replacement of Al by Fe can be also confirmed by lower intensities of the structural diffraction maxima of clinoptilolite. A similar effect was obtained by Kessouri et al. [24] after the deposition of iron into an MFI framework. Hence, the noticeably decreased intensity of the reflections for Fe-Clin-3 can be explained by the highest rate of isomorphous substitution or deposition of bulky species of  $\text{Fe}_2\text{O}_3$  on its surface.

### 2.1.2. Textural Properties of the Materials

Low-temperature  $\text{N}_2$  adsorption–desorption isotherms obtained for raw clinoptilolite (Clin), protonated clinoptilolite (H-Clin), and iron-modified zeolite (Fe-Clin-1, Fe-Clin-2, Fe-Clin-3) are presented in Figure 2. Furthermore, pore volume distribution is shown in Figure 3, while the textural and structural parameters of the samples are summarized in Table 2. Raw clinoptilolite demonstrated IV(a) type isotherm with the hysteresis loop H3, according to the IUPAC classification [25]. This isotherm is characteristic of materials with wedge-shaped mesopores and nonrigid aggregates of platelike particles [25,26]. The specific surface area of the nonmodified clinoptilolite is in range of  $16\text{--}30\text{ m}^2\cdot\text{g}^{-1}$ , which

is typical for clinoptilolite [27]. Vassileva and Voikova [26] reported that the relatively low values of specific surface area and pore volume exhibited by nonmodified clinoptilolite are caused by the limited access of  $N_2$  molecules to the internal structure of the zeolite. As a result, the adsorbate was deposited mainly on the external surface of the material. The results of the experiment performed after  $NH_3$ -SCR tests showed that the specific surface area was preserved, even in the case of the catalytic reaction being conducted under severe conditions. After the dealumination procedure, the volume of mesopores in clinoptilolite significantly increased, suggesting the formation of a mesopore system. The isotherms obtained for iron-modified clinoptilolite are characterized by the isotherms of type IV(a), confirming their mesoporous nature. However, the introduction of iron resulted in a change in the shape of the hysteresis loop from H3 to H4 [28]. This result suggests the transformation of wedge-shaped mesopores into slit-shaped ones. Additionally, as presented in Table 2, after modification with iron, the specific surface area, the volume of mesopores, and the average pore diameter decreased due to pore blockage probably caused by the deposition of iron oxide species [29]. Catalysts of Fe-Clin-X series characteristically possess similar pore distribution (Figure 3). For Fe-Clin-X series, a wide bimodal pore distribution—pores with diameters ranging from 10 to 1000 Å and pores with diameters from 1500 to 7000 Å—was observed. However, the porous structure was definitely dominated by pores with diameters ranging from 10 to 1000 Å (mesopores with  $D_{meso}$  in the range of 208–223 Å). Interestingly, multiple impregnations with  $FeSO_4$  did not result in considerable differences between the  $D_{meso}$  values. Nevertheless, the gradual decline of  $V_{meso}$  with the increasing iron content suggested that iron species were effectively deposited in the inner structure of clinoptilolite.

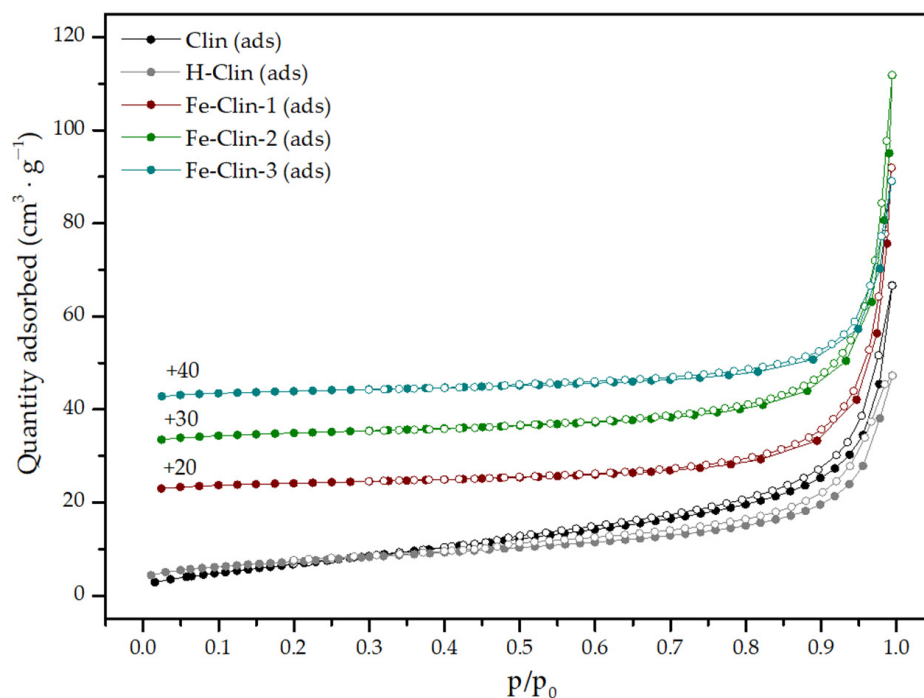


**Figure 2.** Low-temperature  $N_2$  adsorption–desorption isotherms obtained for raw clinoptilolite (Clin) and the investigated catalysts (for better visibility, the isotherms were shifted by the values given in the figure).

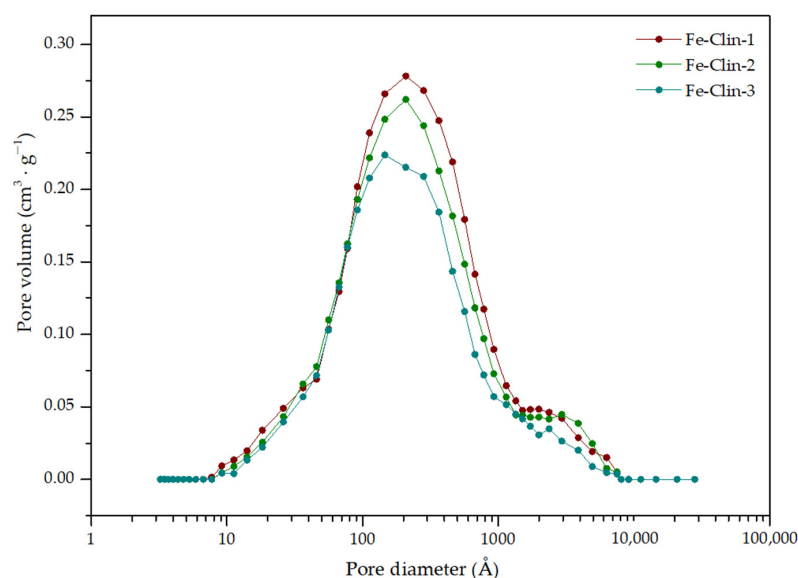


**Figure 3.** Pore volume obtained for Fe-clinoptilolite catalysts.

**Table 2.** Textural and structural parameters of raw clinoptilolite and the Fe-clinoptilolite catalysts.

Sample	$S_{\text{BET}}^{\text{a}}$ ( $\text{m}^2 \cdot \text{g}^{-1}$ )	$S_{\text{Ext}}^{\text{b}}$ ( $\text{m}^2 \cdot \text{g}^{-1}$ )	$V_{\text{meso}}^{\text{c}}$ ( $\text{cm}^3 \cdot \text{g}^{-1}$ )	$D_{\text{meso}}^{\text{c}}$ (nm)
Clin	16	7	0.025	17.0
H-Clin	30	9	0.281	28.2
Fe-Clin-1	15	10	0.277	20.8
Fe-Clin-2	12	13	0.262	20.8
Fe-Clin-3	10	10	0.224	22.3

<sup>a</sup> Specific surface area determined using the BET method; <sup>b</sup> external surface area determined using the t-plot method; <sup>c</sup> average mesopore volume and diameter determined using the BJH method.

### 2.1.3. Characteristic Chemical Groups in the Materials

The FT-IR spectra obtained for the raw and protonated clinoptilolite and the zeolites with various loadings of iron are presented in Figure 4. The characteristic peaks can be divided into three regions: (1) O-H stretching vibrations ( $3800\text{--}3400\text{ cm}^{-1}$ ); (2) Si-O stretching vibrations, Al-Me-OH stretching vibrations, and O-H bending vibrations from  $\text{H}_2\text{O}$  ( $1700\text{--}700\text{ cm}^{-1}$ ); and (3) pseudo lattice vibrations ( $700\text{--}450\text{ cm}^{-1}$ ) [13].

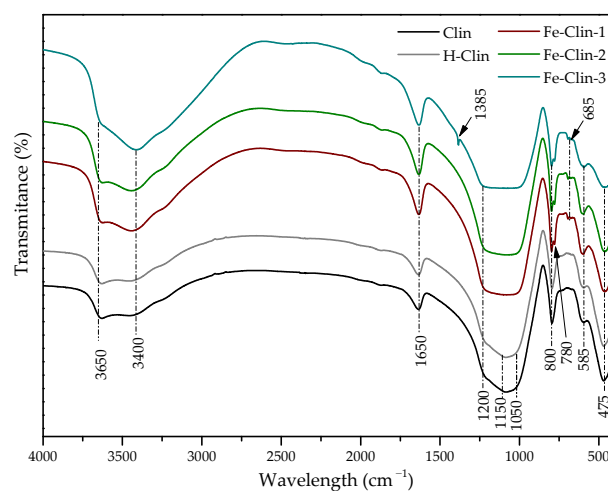


**Figure 4.** FT-IR spectra of raw clinoptilolite (Clin), protonated clinoptilolite (H-Clin), and clinoptilolite modified with different Fe contents (Fe-Clin-1, Fe-Clin-2, Fe-Clin-3).

In the first of the above-mentioned regions, 3800–3400  $\text{cm}^{-1}$ , the shape of the spectra was similar for all of the materials except Fe-Clin-3. The peak at 3650  $\text{cm}^{-1}$  suggested the presence of Brönsted sites provided by the acidic hydroxyl Si-O(H)-Al. In the case of Fe-Clin-3, it was not as sharp as for the other materials; thus, multiple repetition of Fe deposition resulted in the removal of OH groups bonded to the zeolitic structure. The band at 3400  $\text{cm}^{-1}$ , broad for raw and protonated clinoptilolite and sharper for Fe-modified zeolite, corresponded to the vibrations of O-H...O bonds [30].

In the second region of the spectra, 1700–700  $\text{cm}^{-1}$ , the peak at 1650  $\text{cm}^{-1}$ , attributed to deformation vibrations of physisorbed water molecules, showed a similar shape for all materials [31]. However, the characteristic bands at 1200  $\text{cm}^{-1}$  and 1050  $\text{cm}^{-1}$  were almost absent for clinoptilolite modified with Fe. Both of the peaks were related to Al-O or Si-O asymmetric stretching vibrations; thus, incorporation of iron resulted in structural interruptions, such as the removal of charge-balancing  $\text{Ca}^{2+}$  and  $\text{Mg}^{2+}$ . A similar effect was observed by Cobzaru et al. [32] after the modification of natural clinoptilolite with nitric acid. Since  $\text{FeSO}_4$  is regarded as a strongly acidic medium, our results are in line with this research. Moreover, the band at 1150  $\text{cm}^{-1}$ , intense for Clin and H-Clin, partially disappeared after the introduction of iron. Since the peak corresponds to three-dimensional networks of amorphous Si-O-Si units, the modification procedure could partially remove this phase from natural and protonated zeolite. Additionally, a small peak at 1385  $\text{cm}^{-1}$ , appearing only for Fe-Clin-3 and thus with the highest concentration of iron species, was probably ascribed to sulfate groups bonded to iron ions deposited in the zeolitic structure [33].

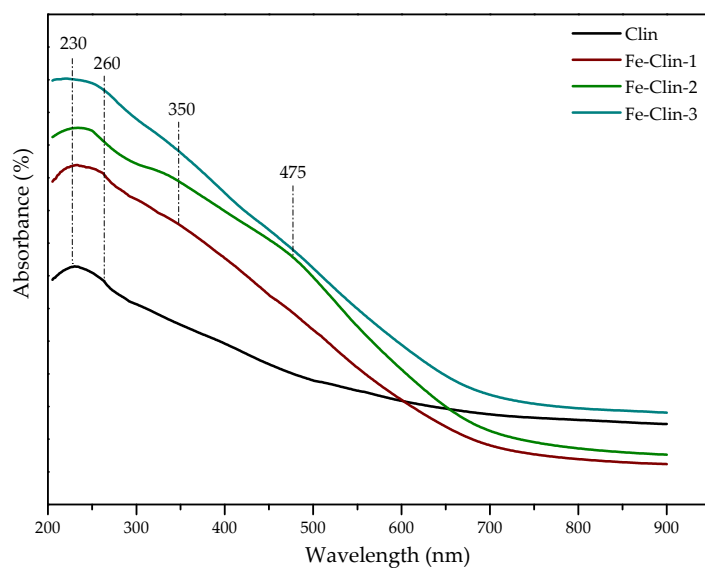
The characteristic peaks detected in the third analyzed region, 700–450  $\text{cm}^{-1}$ , evidenced partial removal of amorphous silica. This effect can be confirmed by the presence of the sharp peaks at 800  $\text{cm}^{-1}$  in the spectra of all the materials. However, after modification with iron, these peaks were noticeably separated. The new small peak at 780  $\text{cm}^{-1}$ , formed through this division, raised from the stretching vibrations of  $[\text{SiO}_4]$  tetrahedra from the zeolitic framework. Therefore, removal of the amorphous silica could enhance the detection of structural peaks of the materials. Another difference in the spectra of iron-modified clinoptilolite compared to the raw or protonated form was the presence of low-intense peaks at 585  $\text{cm}^{-1}$ , which corresponded to the symmetric stretching vibrations of  $[\text{AlO}_4]$  tetrahedra [34]. Two bands at 600  $\text{cm}^{-1}$  and 475  $\text{cm}^{-1}$  were related to O-Al-O or O-Si-O bending vibrations and Si-O stretching vibrations, respectively [35].

#### 2.1.4. Speciation of the Active Phase

The comparative UV-Vis spectra of the raw clinoptilolite and the catalysts with various contents of iron are presented in Figure 5.

In general, for iron-modified zeolites, three main regions in UV-Vis spectra are expected: (1) bands below 300 nm, corresponding to the oxygen-to-metal charge transfer (CT), assigned to isolated framework and extra framework pseudotetrahedral  $\text{Fe}^{3+}$  species; (2) bands in the range of 300–500 nm, related to oligomeric  $\text{Fe}_x\text{O}_y$  or  $\text{Fe}_2\text{O}_3$  nanoparticles; and (3) bands detected above 500 nm, assigned to  $\text{Fe}_2\text{O}_3$  clusters on the external surface of the support [19].

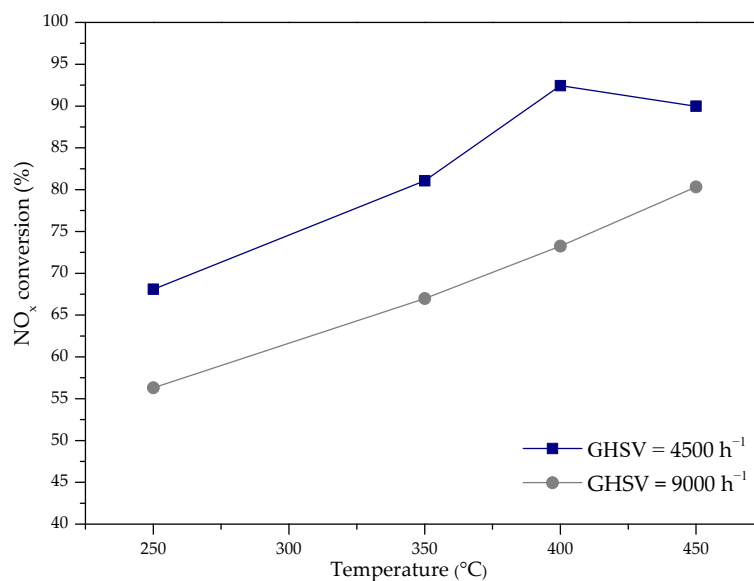
The speciation of iron in the analyzed materials was strongly correlated with the metal loading. As presented in Figure 5, all the investigated samples, including nonmodified clinoptilolite, showed absorption bands at 230 and 260 nm. This result confirmed that iron was originally present (Clin) or isomorphously deposited (Fe-Clin-1, 2, and 3) in the zeolite structure in the form of extraframework cations with octahedral coordination [36]. Furthermore, the band at 350 nm, detected only for the zeolite modified with iron, corresponded to small, oligonuclear clusters of iron oxide [37]. The bands at 475 nm, characteristic of bigger particles of  $\text{Fe}_2\text{O}_3$ , were observed for the samples with increased iron content (Fe-Clin-2, Fe-Clin-3). Therefore, the extraframework phase of  $\text{Fe}_2\text{O}_3$  became dominant as a result of the increase in iron loading due to the agglomeration of the species into bigger particles.



**Figure 5.** UV-Vis spectra of raw clinoptilolite (Clin) and clinoptilolite modified with different Fe contents (Fe-Clin-1, Fe-Clin-2, Fe-Clin-3).

## 2.2. $\text{NH}_3$ -SCR Catalytic Tests Performed with Industrial Gas Mixture

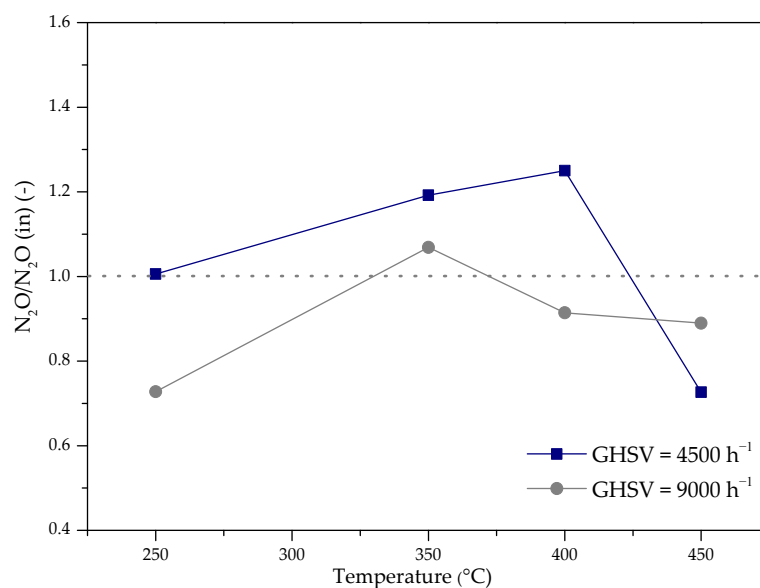
$\text{NH}_3$ -SCR catalytic tests over protonated clinoptilolite were conducted under the conditions reflecting that of industrial nitric acid plant (regarding catalytic bed loading and temperature range). The obtained results are presented in Figure 6. The tests were carried out at two catalytic bed loads. It was observed that in both cases,  $\text{NO}_x$  conversion exceeded 50% in the entire temperature range. The maximum conversion of more than 90%, was reached above 400 °C, and higher  $\text{NO}_x$  conversion was achieved for the lower catalytic bed loading. In the case of  $\text{GHSV} = 4500 \text{ h}^{-1}$  (tail gas flow  $0.15 \text{ Nm}^3 \cdot \text{h}^{-1}$ ), 93% of  $\text{NO}_x$  conversion was obtained at 400 °C. On the other hand, for  $\text{GHSV} = 9000 \text{ h}^{-1}$  (tail gas flow  $0.3 \text{ Nm}^3 \cdot \text{h}^{-1}$ ), the material exhibited 80% of  $\text{NO}_x$  conversion at 450 °C.



**Figure 6.**  $\text{NO}_x$  conversion as a function of temperature and catalyst load for H-Clin.

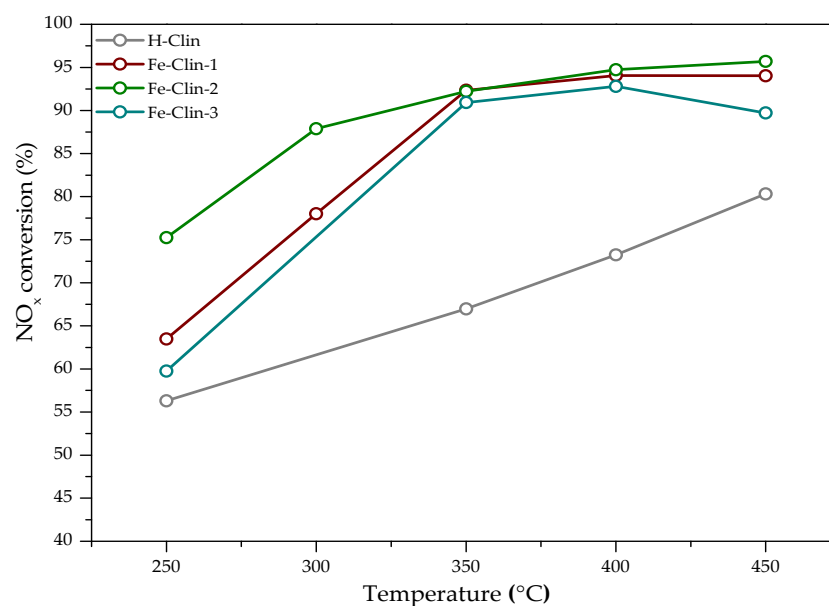
During the test,  $\text{N}_2\text{O}$  concentration upstream and downstream of the catalytic bed was measured as well. The dash line in Figure 7 represents the ratio of the  $\text{N}_2\text{O}$  concentration downstream to the inlet concentration of  $\text{N}_2\text{O}$ . It was clearly indicated that higher loading of the catalytic bed resulted in lower  $\text{N}_2\text{O}$  concentration downstream of the bed compared to

the inlet concentration of  $N_2O$ . This effect was observed over almost the entire investigated temperature range. Moreover, regardless of the catalytic bed load, the highest selectivity was observed at 450 °C.



**Figure 7.**  $N_2O/N_{2O(in)}$  ratio as a function of temperature and catalyst load for H-Clin.

Figure 8 shows the results of the catalytic tests obtained for iron-modified samples and the protonated clinoptilolite, while the selectivity of the materials to  $N_2$  is listed in Table 3. In all cases,  $NO_x$  conversion of iron-modified zeolite was higher than that of H-Clin. Above 350 °C, regardless of the iron content in the sample,  $NO_x$  conversion of over 90% was achieved. The highest activity in the entire temperature range was exhibited by Fe-Clin-2. Additionally, selectivity of Fe-clinoptilolite catalysts to  $N_2$  was in the range of 93–100%, confirming the negligible contribution of the side reactions to the whole mechanism of  $NH_3$ -SCR performed on the materials.

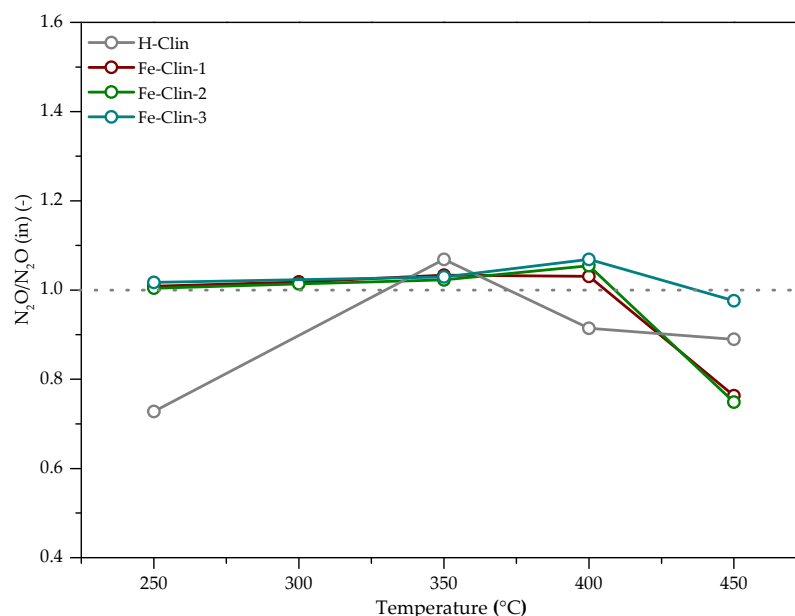


**Figure 8.**  $NO_x$  conversion as a function of temperature for protonated clinoptilolite (H-Clin) and Fe-clinoptilolite catalysts (Fe-Clin-1, Fe-Clin-2, Fe-Clin-3) at  $GHSV = 9000 h^{-1}$ .

**Table 3.** N<sub>2</sub> selectivity of Fe-clinoptilolite catalysts.

Sample	Selectivity Towards N <sub>2</sub> (%)				
	250 °C	300 °C	350 °C	400 °C	450 °C
Fe-Clin-1	99.2	98.2	96.7	96.9	100.0
Fe-Clin-2	99.6	98.6	97.7	94.6	100.0
Fe-Clin-3	98.3	-	97.1	93.1	100.0

The N<sub>2</sub>O concentrations measured during the experiments are shown in Figure 9. In the case of protonated clinoptilolite, the N<sub>2</sub>O concentration increased above the inlet value only at 350 °C. For iron-modified samples, the courses of the curves are similar to each other. Up to the temperature of 400 °C, the concentration of N<sub>2</sub>O behind the bed slightly increased in relation to the initial concentration ( $N_2O/N_{2O(in)} > 1$ ), and then, a sharp decrease in the concentration of N<sub>2</sub>O at the temperature of 450 °C was noted. The greatest decrease was obtained for the Fe-Clin-1 and Fe-Clin-2 samples. Overall, satisfactory catalytic performance exhibited by the investigated catalysts confirmed that one or two iron impregnations of clinoptilolite are sufficient to obtain an effective NH<sub>3</sub>-SCR catalyst.

**Figure 9.** The ratio of N<sub>2</sub>O concentration downstream of the catalytic bed and N<sub>2</sub>O inlet concentration as a function of the temperature for H-Clin, Fe-Clin-1, Fe-Clin-2, Fe-Clin-3 at GHSV = 9000 h<sup>-1</sup>.

### 3. Materials and Methods

#### 3.1. Catalysts Preparation

The precursor of the investigated catalysts was raw zeolite with a high content of clinoptilolite phase. Firstly, the material was dealuminated using 5% HNO<sub>3</sub> solution. The operation was repeated three times in order to increase the dealumination rate. After each dealumination step, the precursor was washed with demineralized water until pH was <6 and dried at 105–110 °C. Subsequently, the zeolite was fractionated into 0.3–0.8 mm grains and formed into pellets of 5.0 × 4.8 mm dimensions, illustrated in Figure 10. Afterwards, the materials were calcined at 450 °C for 2 h. Iron-modified materials were prepared using the wet impregnation method using an aqueous solution of 1 M FeSO<sub>4</sub> as Fe precursor. The samples were left in contact with the solution at 50 °C for 1 h, then dried at 105–110 °C and calcined at 500 °C for 2 h. The impregnation procedure was performed one, two, or three times in order to obtain catalysts with various Fe loadings. The precursors were dried and calcined before each impregnation treatment. The preparation procedure is schematically illustrated in Figure 10.

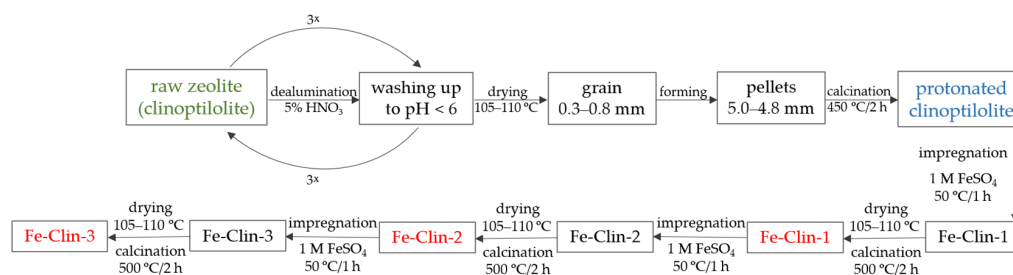


**Figure 10.** Schematic preparation procedure of Fe-clinoptilolite catalysts.

The formed samples of protonated clinoptilolite and Fe-clinoptilolite catalysts, prepared on a laboratory scale, are presented in Figure 11A,B, respectively. The codes of the samples with the corresponding descriptions are listed in Table 4.

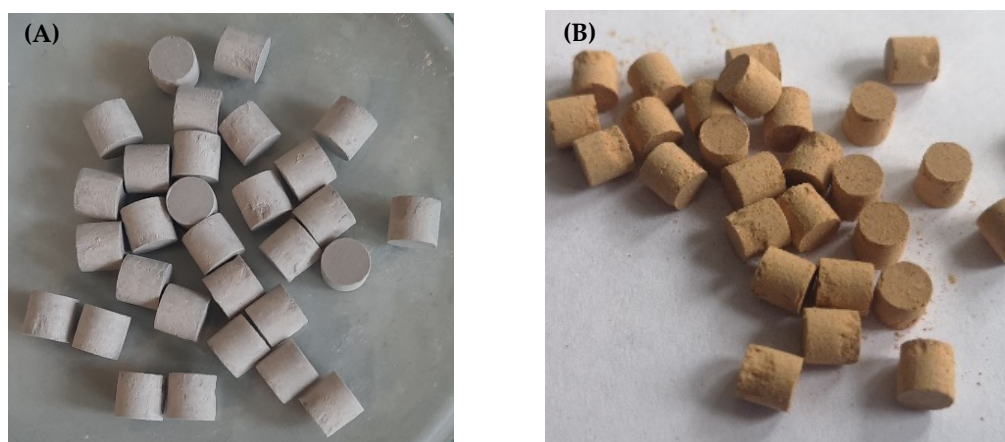


**Figure 11.** Protonated clinoptilolite (A) and Fe-clinoptilolite catalyst formed into pellets (B).

**Table 4.** The list of the samples with their codes and descriptions.

Sample	Description of the Sample
Clin	Raw clinoptilolite
H-Clin	Protonated clinoptilolite
Fe-Clin-1	The catalyst obtained by single impregnation with Fe precursor
Fe-Clin-2	The catalyst obtained by dual impregnation with Fe precursor
Fe-Clin-3	The catalyst obtained by triple impregnation with Fe precursor

### 3.2. Catalysts Characterization

X-ray fluorescence (XRF) was used to determine the chemical composition of the samples using Energy Dispersive X-ray Fluorescence EDXRF Spectrometer, Epsilon 3XLE PANalytical Company. The crystalline structure of the samples was analyzed using an X-ray diffraction (XRD) technique. X-ray diffraction patterns were obtained using an Empyrean diffractometer (Panalytical) equipped with a copper-based anode (Cu-K $\alpha$  LFF HR,  $\lambda = 0.154059$  nm). The measurement was conducted in the  $2\theta$  range of  $2.0$ – $70.0^\circ$  ( $2\theta$  step scans of  $0.02^\circ$  and the counting time of 1 s per step). The specific surface area, total pore volume, and mesopore volume were determined using an ASAP<sup>®</sup> 2050 Xtended Pressure sorption analyzer (Micromeritics Instrument Co., Norcross, GA, USA) based on N<sub>2</sub> adsorption–desorption isotherms at  $-196$  °C using the BET adsorption model (Brunauer–Emmett–Teller) and the BJH transformation (Barret–Joyner–Halenda). Fourier transform infrared spectroscopy studies (FT-IR) were conducted using a Perkin Elmer Frontier FT-IR spectrometer. The spectra were obtained in the wavelength range of  $4000$ – $400$  cm<sup>-1</sup> with a resolution of  $4$  cm<sup>-1</sup>. Before each measurement, the sample was mixed with KBr in a ratio of 1:100 and pressed into a disk. Coordination and aggregation of iron species were

determined by UV–Vis spectroscopy at a wavelength range of 200–900 nm with a resolution of 1 nm using a Perkin Elmer Lambda 35 UV–Vis spectrophotometer.

### 3.3. Catalytic Tests in Real Gas Conditions

The activity and selectivity of the catalysts in the  $\text{NH}_3$ -SCR process were tested in the laboratory installation in the flow of the tail gases stream derived from the pilot ammonia oxidation plant. The laboratory installation consisted of a reactor (R) with a diameter of 25 mm and heat exchangers (HEX and  $\text{HEX}_{\text{NH}_3}$ ) used for preheating tail gases and ammonia. In the tests, the height of the catalyst layer was 70 mm. The installation is schematically presented in Figure 12. The heated tail gases were mixed with ammonia and turned into the catalytic bed. The composition of the tail gases was similar to the tail gases emitted from industrial nitric acid plants; consisted of NO,  $\text{NO}_2$ ,  $\text{N}_2\text{O}$ ,  $\text{O}_2$ ,  $\text{N}_2$ , and  $\text{H}_2\text{O}$ ; and contained approximately 900–1100 ppm of  $\text{NO}_x$ , ( $\text{NO}/\text{NO}_2 = 2\text{--}2.6$ ) 400–600 ppm of  $\text{N}_2\text{O}$ , 2–3 vol.% of  $\text{O}_2$ , and 0.3–0.5 vol.% of  $\text{H}_2\text{O}$ . The amount of  $\text{NH}_3$  used in the reaction was increased and optimized to the level providing maximum  $\text{NO}_x$  conversion with minimal  $\text{NH}_3$  slip (less than 10 ppm). Thus, the  $\text{NH}_3$  concentration was maintained at 0.14–0.15 vol.%, depending on the inlet  $\text{NO}_x$  concentration.

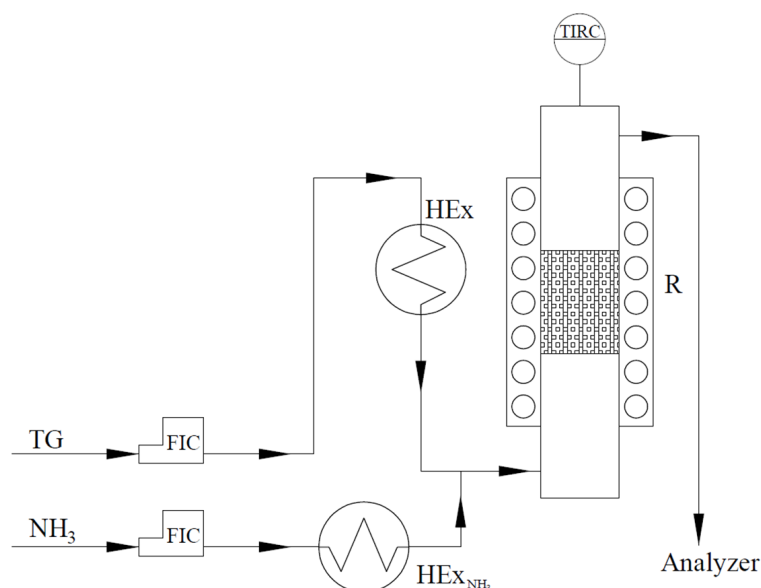


**Figure 12.** The scheme of the laboratory installation for  $\text{NH}_3$ -SCR catalytic tests.

In each test, 30 g of the catalyst in a form of pellet ( $d = 5.0 \times 4.8$  mm) was placed into the reactor. The activity studies were performed at 250, 300, 350, 400, and 450 °C. The temperature inside the reactor was controlled by a thermocouple installed at the gas outlet from the bed. The research was conducted in  $\text{GHSV} = 4500$  and  $9000 \text{ h}^{-1}$  (tail gas flow  $0.15$  and  $0.3 \text{ Nm}^3 \cdot \text{h}^{-1}$ , respectively). Temperature, GHSV, and shape of catalyst were selected to be as close as possible to conditions prevailing in industrial plants. The measurements of the inlet and outlet concentrations of NO,  $\text{NO}_2$ ,  $\text{N}_2\text{O}$ , and  $\text{NH}_3$  were conducted at each temperature after stabilizing the equilibrium conditions and operating parameters. The concentrations of unreacted NO,  $\text{NO}_2$ , and  $\text{N}_2\text{O}$  were analyzed downstream of the reactor by a GASMET FT-IR analyzer (Vantaa, Finland).  $\text{NO}_x$  reduction was important in this study; thus, NO and  $\text{NO}_2$  concentrations were not considered separately.  $\text{NO}_x$  conversion was calculated according to Equation (6):

$$X_{\text{NO}_x} = \frac{\text{NO}_x(\text{in}) - \text{NO}_x}{\text{NO}_x(\text{in})} \cdot 100\% \quad (6)$$

where  $X_{\text{NO}_x}$ — $\text{NO}_x$  conversion,  $\text{NO}_x(\text{in})$ —inlet concentration of  $\text{NO}_x$ , while  $\text{NO}_x$ — $\text{NO}_x$  concentration in the gas after catalytic reaction.

#### 4. Conclusions

This paper has demonstrated the catalytic potential of protonated or protonated and iron-modified clinoptilolite in the form of pellets in  $\text{NH}_3$ -SCR within the range of 250–450 °C. Pretreatment with  $\text{HNO}_3$  and deposition of iron changed the shape of mesopores and resulted in the formation of secondary porosity. Additionally, deposition of iron caused some interruptions in the order of the zeolite framework. Nevertheless, the crystallinity was not affected by the performed modifications. Catalytic tests were conducted using a gas mixture which reflected industrial conditions. For H-Clin, the maximum conversion of  $\text{NO}_x$  of over 90% was achieved above 400 °C and  $\text{GHSV} = 4500 \text{ h}^{-1}$ . At the load of  $9000 \text{ h}^{-1}$ , the conversion of  $\text{NO}_x$  reached more than 60% in the entire temperature range. Satisfactory results obtained for the protonated zeolite without the addition of the active phase can be explained by the natural presence of iron species in the clinoptilolite structure. Regardless of iron loading,  $\text{NO}_x$  conversion obtained for the catalysts was higher than that of the H-Clin. In the case of Fe-Clin-1 and Fe-Clin-2,  $\text{NO}_x$  conversion exceeded 90% above 350 °C. Slightly lower  $\text{NO}_x$  reduction was recorded for Fe-Clin-3. In summary, it was demonstrated that even a single impregnation of natural zeolite (Fe-Clin-1) resulted in the satisfactory catalytic performance, since more than 90% of  $\text{NO}_x$  conversion was achieved between 350–450 °C. Additionally, it was noted that  $\text{N}_2\text{O}$  concentration decreased by 20% compared to the initial concentration. The strength and significance of our work lies especially in the minimization of the catalyst preparation steps, which is highly beneficial from technological and economical points of view. In summary, it was demonstrated that Fe-clinoptilolite catalysts are advantageous, low-cost, and easy-to-prepare materials that exhibit satisfactory features in the  $\text{NH}_3$ -SCR process.

**Author Contributions:** Conceptualization, M.S., M.M. and M.I.; methodology, M.S. and M.I.; resources, K.A.-J.; investigations, M.S. and A.S.-W.; writing—original draft preparation, M.S. and A.S.-W.; writing—review and editing, M.I. and B.S.; supervision, M.I., M.M. and B.S. All authors have read and agreed to the published version of the manuscript.

**Funding:** M.S. acknowledges the financial support to the program of the Ministry of Science and Higher Education entitled “Implementation Doctorate”.

**Acknowledgments:** A.S.-W. gratefully acknowledges financial support from the National Science Centre Grant Preludium 19 (no. 2020/37/N/ST5/00186) The research results presented by M.M. have been developed with the use of equipment financed from the funds of the “Excellence Initiative—Research University” program at AGH University of Science and Technology. B.S.’s research project was partly supported by the program “Excellence initiative—research university” for the AGH University of Science and Technology”.

**Conflicts of Interest:** The authors declare no conflict of interest. The funders had no role in the design of the study; in the collection, analyses, or interpretation of data; in the writing of the manuscript; or in the decision to publish the results.

#### References

1. Forzatti, P. Present Status and Perspectives in De- $\text{NO}_x$  SCR Catalysis. *Appl. Catal. A Gen.* **2001**, *222*, 221–236. [[CrossRef](#)]
2. European Commission. *Integrated Pollution Prevention and Control Reference Document on Best Available Techniques for the Manufacture of Large Volume Inorganic Chemicals—Ammonia, Acids and Fertilisers*; European Commission: Brussels, Belgium, 2007.
3. Kwon, D.W.; Park, K.H.; Ha, H.P.; Hong, S.C. The Role of Molybdenum on the Enhanced Performance and  $\text{SO}_2$  Resistance of V/Mo-Ti Catalysts for  $\text{NH}_3$ -SCR. *Appl. Surf. Sci.* **2019**, *481*, 1167–1177. [[CrossRef](#)]
4. Damma, D.; Ettireddy, P.R.; Reddy, B.M.; Smirniotis, P.G. A Review of Low Temperature  $\text{NH}_3$ -SCR for Removal of  $\text{NO}_x$ . *Catalysts* **2019**, *9*, 349. [[CrossRef](#)]
5. Liu, Q.; Bian, C.; Ming, S.; Guo, L.; Zhang, S.; Pang, L.; Liu, P.; Chen, Z.; Li, T. The Opportunities and Challenges of Iron-Zeolite as  $\text{NH}_3$ -SCR Catalyst in Purification of Vehicle Exhaust. *Appl. Catal. A Gen.* **2020**, *607*, 117865. [[CrossRef](#)]
6. Husnain, N.; Wang, E.; Li, K.; Anwar, M.T.; Mehmood, A.; Gul, M.; Li, D.; Mao, J. Iron Oxide-Based Catalysts for Low-Temperature Selective Catalytic Reduction of  $\text{NO}_x$  with  $\text{NH}_3$ . *Rev. Chem. Eng.* **2019**, *35*, 239–264. [[CrossRef](#)]

7. Wu, X.; Liu, J.; Liu, X.; Wu, X.; Du, Y. Fabrication of Carbon Doped Cu-Based Oxides as Superior NH<sub>3</sub>-SCR Catalysts via Employing Sodium Dodecyl Sulfonate Intercalating CuMgAl-LDH. *J. Catal.* **2022**, *407*, 265–280. [[CrossRef](#)]
8. Kobayashi, M.; Kuma, R.; Masaki, S.; Sugishima, N. TiO<sub>2</sub>-SiO<sub>2</sub> and V<sub>2</sub>O<sub>5</sub>/TiO<sub>2</sub>-SiO<sub>2</sub> Catalyst: Physico-Chemical Characteristics and Catalytic Behavior in Selective Catalytic Reduction of NO by NH<sub>3</sub>. *Appl. Catal. B Environ.* **2005**, *60*, 173–179. [[CrossRef](#)]
9. Han, L.; Cai, S.; Gao, M.; Hasegawa, J.Y.; Wang, P.; Zhang, J.; Shi, L.; Zhang, D. Selective Catalytic Reduction of NO<sub>x</sub> with NH<sub>3</sub> by Using Novel Catalysts: State of the Art and Future Prospects. *Chem. Rev.* **2019**, *119*, 10916–10976. [[CrossRef](#)]
10. Zhu, J.; Liu, Z.; Xu, L.; Ohnishi, T.; Yanaba, Y.; Ogura, M.; Wakihara, T.; Okubo, T. Understanding the High Hydrothermal Stability and NH<sub>3</sub>-SCR Activity of the Fast-Synthesized ERI Zeolite. *J. Catal.* **2020**, *391*, 346–356. [[CrossRef](#)]
11. Ambrozova, P.; Kynicky, J.; Urubek, T.; Nguyen, V.D. Synthesis and Modification of Clinoptilolite. *Molecules* **2017**, *22*, 1107. [[CrossRef](#)]
12. Szymaszek-Wawryca, A.; Díaz, U.; Samojeden, B.; Motak, M. Catalytic Performance of One-Pot Synthesized Fe-MWW Layered Zeolites (MCM-22, MCM-36, and ITQ-2) in Selective Catalytic Reduction of Nitrogen Oxides with Ammonia. *Molecules* **2022**, *27*, 2983. [[CrossRef](#)]
13. Szymaszek, A.; Samojeden, B.; Motak, M. Selective Catalytic Reduction of NO<sub>x</sub> with Ammonia (NH<sub>3</sub>-SCR) over Transition Metal-Based Catalysts-Influence of the Catalysts Support. *Physicochem. Probl. Miner. Process.* **2019**, *55*, 1429–1441. [[CrossRef](#)]
14. Dakdareh, A.M.; Falamaki, C.; Ghasemian, N. Hydrothermally Grown Nano-Manganese Oxide on Clinoptilolite for Low-Temperature Propane-Selective Catalytic Reduction of NO<sub>x</sub>. *J. Nanoparticle Res.* **2018**, *20*, 309. [[CrossRef](#)]
15. Ghasemian, N.; Falamaki, C.; Kalbasi, M.; Khosravi, M. Enhancement of the Catalytic Performance of H-Clinoptilolite in Propane-SCR-NO<sub>x</sub> Process through Controlled Dealumination. *Chem. Eng. J.* **2014**, *252*, 112–119. [[CrossRef](#)]
16. Ghasemian, N.; Nourmoradi, H. The Study of the Performance of Iranian Clinoptilolite Zeolite in Removal of Nitrogen Oxide (NO<sub>x</sub>) from Stack of Industries by Using Selective Catalytic Reduction System (SCR). *J. Ilam Univ. Med. Sci.* **2015**, *23*, 27–35.
17. Ghasemian, N.; Falamaki, C.; Kalbasi, M. Clinoptilolite Zeolite as a Potential Catalyst for Propane-SCR-NO<sub>x</sub>: Performance Investigation and Kinetic Analysis. *Chem. Eng. J.* **2014**, *236*, 464–470. [[CrossRef](#)]
18. Saramok, M.; Szymaszek, A.; Inger, M.; Antoniak-Jurak, K.; Samojeden, B.; Motak, M. Modified Zeolite Catalyst for a NO<sub>x</sub> Selective Catalytic Reduction Process in Nitric Acid Plants. *Catalysts* **2021**, *11*, 450. [[CrossRef](#)]
19. Boroń, P.; Chmielarz, L.; Gurgul, J.; Łątka, K.; Gil, B.; Marszałek, B.; Dzwigaj, S. Influence of Iron State and Acidity of Zeolites on the Catalytic Activity of FeHBEA, FeHZSM-5 and FeHMOR in SCR of NO with NH<sub>3</sub> and N<sub>2</sub>O Decomposition. *Microporous Mesoporous Mater.* **2015**, *203*, 73–85. [[CrossRef](#)]
20. Zhang, T.; Qin, X.; Peng, Y.; Wang, C.; Chang, H.; Chen, J.; Li, J. Effect of Fe Precursors on the Catalytic Activity of Fe/SAPO-34 Catalysts for N<sub>2</sub>O Decomposition. *Catal. Commun.* **2019**, *128*, 105706. [[CrossRef](#)]
21. Burris, L.E.; Juenger, M.C. The Effect of Acid Treatment on the Reactivity of Natural Zeolites Used as Supplementary Cementitious Materials. *Cem. Concr. Res.* **2016**, *79*, 185–193. [[CrossRef](#)]
22. Lin, H.; Liu, Q.L.; Dong, Y.B.; He, Y.H.; Wang, L. Physicochemical Properties and Mechanism Study of Clinoptilolite Modified by NaOH. *Microporous Mesoporous Mater.* **2015**, *218*, 174–179. [[CrossRef](#)]
23. Xu, S.; Habib, A.H.; Gee, S.H.; Hong, Y.K.; McHenry, M. Spin Orientation, Structure, Morphology, and Magnetic Properties of Hematite Nanoparticles. *J. Appl. Phys.* **2015**, *117*, 17A315. [[CrossRef](#)]
24. Kessouri, A.; Boukoussa, B.; Bengueddach, A.; Hamacha, R. Synthesis of Iron-MFI Zeolite and Its Photocatalytic Application for Hydroxylation of Phenol. *Res. Chem. Intermed.* **2018**, *44*, 2475–2487. [[CrossRef](#)]
25. Thommes, M.; Kaneko, K.; Neimark, A.V.; Olivier, J.P.; Rodriguez-Reinoso, F.; Rouquerol, J.; Sing, K.S.W. Physisorption of Gases, with Special Reference to the Evaluation of Surface Area and Pore Size Distribution (IUPAC Technical Report). *Pure Appl. Chem.* **2015**, *87*, 1051–1069. [[CrossRef](#)]
26. Vassileva, P.; Voikova, D. Investigation on Natural and Pretreated Bulgarian Clinoptilolite for Ammonium Ions Removal from Aqueous Solutions. *J. Hazard. Mater.* **2009**, *170*, 948–953. [[CrossRef](#)]
27. Doula, M.K. Synthesis of a Clinoptilolite-Fe System with High Cu Sorption Capacity. *Chemosphere* **2007**, *67*, 731–740. [[CrossRef](#)]
28. Yang, Y.; Gu, Y.; Lin, H.; Jie, B.; Zheng, Z.; Zhang, X. Bicarbonate-Enhanced Iron-Based Prussian Blue Analogs Catalyze the Fenton-like Degradation of p-Nitrophenol. *J. Colloid Interface Sci.* **2022**, *608*, 2884–2895. [[CrossRef](#)]
29. Rutkowska, M.; Díaz, U.; Palomares, A.E.; Chmielarz, L. Cu and Fe Modified Derivatives of 2D MWW-Type Zeolites (MCM-22, ITQ-2 and MCM-36) as New Catalysts for DeNO<sub>x</sub> Process. *Appl. Catal. B Environ.* **2015**, *168–169*, 531–539. [[CrossRef](#)]
30. Korkuna, O.; Leboda, R.; Skubiszewska-Zięba, J.; Vrublevs'ka, T.; Gun'ko, V.M.; Ryczkowski, J. Structural and Physicochemical Properties of Natural Zeolites: Clinoptilolite and Mordenite. *Microporous Mesoporous Mater.* **2006**, *87*, 243–254. [[CrossRef](#)]
31. Kumar, A.; Lingfa, P. Sodium Bentonite and Kaolin Clays: Comparative Study on Their FT-IR, XRF, and XRD. *Mater. Today Proc.* **2019**, *22*, 737–742. [[CrossRef](#)]
32. Cobzaru, C.; Marinoiu, A.; Cernatescu, C. Sorption of Vitamin C on Acid Modified Clinoptilolite. *Rev. Roum. Chim.* **2015**, *60*, 241–247.
33. Long, R.; Yang, R. Characterization of Fe-ZSM-5 Catalyst for Selective Catalytic Reduction of Nitric Oxide by Ammonia. *J. Catal.* **2000**, *194*, 80–90. [[CrossRef](#)]
34. Doula, M.K.; Ioannou, A. The Effect of Electrolyte Anion on Cu Adsorption-Desorption by Clinoptilolite. *Microporous Mesoporous Mater.* **2003**, *58*, 115–130. [[CrossRef](#)]

35. Hayati-Ashtiani, M. Use of FTIR Spectroscopy in the Characterization of Natural and Treated Nanostructured Bentonites (Montmorillonites). *Part. Sci. Technol.* **2012**, *30*, 553–564. [[CrossRef](#)]
36. Grzybek, J.; Gil, B.; Roth, W.J.; Skoczek, M.; Kowalczyk, A.; Chmielarz, L. Spectrochimica Acta Part A: Molecular and Biomolecular Spectroscopy Characterization of Co and Fe-MCM-56 Catalysts for NH<sub>3</sub>-SCR and N<sub>2</sub>O Decomposition: An in Situ FTIR Study. *Spectrochim. Acta Part A Mol. Biomol. Spectrosc.* **2018**, *196*, 281–288. [[CrossRef](#)]
37. Rivas, F.C.; Rodriguez-Iznaga, I.; Berlier, G.; Ferro, D.T.; Conception-Rosabal, B.; Pertanovskii, V. Fe Speciation in Iron Modified Natural Zeolites as Sustainable Environmental Catalysts. *Catalysts* **2019**, *9*, 866. [[CrossRef](#)]